

On the origin of the cusp in the transverse momentum distribution for the process of strong field ionization.

I. A. Ivanov^{1,2*}

¹*Center for Relativistic Laser Science, Institute for Basic Science,
Gwangju 500-712, Republic of Korea and*

²*Research School of Physics and Engineering,*

The Australian National University, Canberra ACT 0200, Australia

(Dated: February 4, 2019)

We study the origin of the cusp-structure in the transverse or lateral electron momentum distribution (TEMD) for the process of tunelling ionization driven by a linearly polarized laser pulse. We show that appearance of the cusp in the TEMD can be explained as follows. Projection on the set of the Coulomb scattering states leads to appearance of "elementary" cusps which have simple structure as functions of the lateral momentum. This structure is independent of the detailed dynamics of the ionization process and can be described analytically. These "elementary" cusps can be used to describe the cusp-structure in TEMD.

I. INTRODUCTION

The seminal paper by Keldysh [1] laid out the distinction between tunelling and multi-photon regimes in the photo-ionization process. Particularly fruitful the Keldysh's paradigm proved for the study of the tunelling ionization, a photo-ionization process characterized by the small values of the so-called Keldysh parameter $\gamma = \omega\sqrt{2|\epsilon_0|}/E$ (here ω , E and $|\epsilon_0|$ are the frequency, field strength and ionization potential of the target system expressed in atomic units). Subsequent developments [2–5] elaborated on various aspects of this approach in the tunelling regime, making it an extremely useful and versatile tool for understanding tunelling photo-ionization. Comprehensive reviews of these developments (to which we will be referring below as tunelling theories) can be found in [6, 7].

A remarkable feature of the tunelling regime is that one may still use to some extent the classical

*Electronic address: Igor.Ivanov@anu.edu.au

notions, such as that of the electron trajectory. This fact has been extensively used in the modeling of the tunelling photo-ionization. In this approach tunelling photo-ionization is regarded as a process in which electron first emerges into the continuum as a result of the under-the-barrier tunelling. This part of the problem is described quantum mechanically, producing probabilistic distributions of the electron's characteristics (typically velocities), which can be used as initial conditions for the subsequent classical modeling describing electron motion after the ionization event. Such a procedure has been used with success to produce ionization spectra in good agreement with experiment [8] for complicated systems where truly *ab initio* treatment becomes hopelessly complicated.

These distributions which weight different initial conditions in the electron's phase space are not themselves observed in the experiment. The electron momentum distribution measured at the detector can, however, provide an information about the distributions at the moment of the ionization event, which offers an exciting possibility to look at this event experimentally [9, 10]. Of course, from the strict quantum-mechanical point of view the notion of the electron escaping the atom at a particular moment of time should be regarded with some caution [11]), nevertheless, this picture of electron escaping into the continuum proved extremely fruitful.

Tunelling theories predict simple Gaussian-like structures for these initial distributions. If the after-ionization-event motion is treated as guided by the laser field only (ionic core potential is neglected), the momentum distributions at the detector retains this Gaussian character, with a possible shift of the distribution in the momentum space due to the overall momentum electron acquires from the laser field after the ionization event [6]. Of particular interest, therefore, is the so-called transverse or lateral electron momentum distribution (TEMD), which describes the distribution of the electron momenta measured at the detector in the direction perpendicular to the polarization plane of the driving pulse. In the simple picture when electron motion is guided by the laser field only, the TEMD is unaffected by the motion subsequent to the ionization event.

This prediction is not always true. While the TEMD measured at the detector is a Gaussian for the driving pulse with close to circular polarization [12], it looks rather different for the case of the linear polarization. It has been found [13] that for the case of the linearly polarized laser pulse the transverse electron momentum distribution exhibits a sharp cusp-like peak at zero transverse momentum. We studied this transition from the cusp-like to the Gaussian-like structure in TEMD numerically using the *ab initio* solution of the time-dependent Schrödinger equation (TDSE) in [14].

Study of the TEMD can provide other useful information. It has been demonstrated, both experimentally and theoretically [15], that the transverse electron momentum distributions in the tunneling and over the barrier ionization regimes (OBI) evolve in markedly different ways when the ellipticity parameter describing polarization state of the driving laser pulse increases. This fact can be used to make a clear distinction between the tunneling and OBI regimes in the experiment.

In the present work we study the origin of the cusp-structure in TEMD for the case of the linearly polarized driving laser pulse in detail. In [13] this structure at zero transverse momentum has been attributed to low-energy singularity of the Coulomb wave-function [13]. We show that though this interpretation is basically correct there is more to the story. Projection on the set of the Coulomb scattering states produces the "elementary" cusps which have simple structure as functions of the lateral momentum. This structure can be described analytically. These "elementary" cusps can be used to describe the cusp-structure in TEMD.

II. THEORY AND RESULTS

We will be guided below to a considerable extent by the numerical results provided by the solution of the TDSE for a hydrogen atom. We will briefly describe the procedure, therefore. We solve TDSE for a hydrogen atom in presence of a laser pulse:

$$i\frac{\partial\Psi(\mathbf{r})}{\partial t} = (\hat{H}_{\text{atom}} + \hat{H}_{\text{int}}(t))\Psi(\mathbf{r}). \quad (1)$$

Operator $\hat{H}_{\text{int}}(t)$ in Eq. (1) describes interaction of the atom with the EM field. We use velocity form for this operator:

$$\hat{H}_{\text{int}}(t) = \mathbf{A}(t) \cdot \hat{\mathbf{p}}, \quad (2)$$

with

$$\mathbf{A}(t) = -\int_0^t \mathbf{E}(\tau) d\tau. \quad (3)$$

The laser pulse is linearly polarized along the z -direction, which we use as a quantization axis:

$$E_z = E_0 f(t) \cos \omega t \quad (4)$$

For the base frequency of the pulse we use $\omega = 0.057$ a.u. (corresponding to the wavelength of 790 nm). The function $f(t) = \sin^2(\pi t/T_1)$ in Eq. (4) (here $T_1 = NT$ is a total pulse duration, N

is an integer, $T = 2\pi/\omega$ is an optical cycle of the field). We report below results for various pulse durations T_1 and field strengths E_0 . TDSE is solved for a time interval $(0, T_1)$. Initial state of the system is a ground state of the hydrogen atom.

To solve the TDSE we employed the procedure described in the works [16, 17]. Solution of the TDSE is represented as a series in spherical harmonics:

$$\Psi(\mathbf{r}, t) = \sum_{l=0}^{L_{\max}} f_l(r, t) Y_{l0}(\theta). \quad (5)$$

The radial part of the TDSE is discretized on the grid with the step-size $\delta r = 0.1$ a.u. in a box of the size $R_{\max} = 600$ a.u. We consider below relatively short total pulse durations and moderately strong field intensities (not exceeding 6 optical cycles and 3.5×10^{14} W/cm² respectively). We used $L_{\max} = 50$ in the calculations reported below. The necessary checks ensuring that for such field parameters calculation is well converged with respect to L_{\max} and R_{\max} have been performed.

Substitution of the expansion (5) into the TDSE gives a system of coupled equations for the radial functions $f_l(r, t)$. To solve this system we use the matrix iteration method [18]. Ionization amplitudes $a(\mathbf{p})$ are obtained by projecting solution of the TDSE at the end of the laser pulse on the set of the ingoing scattering states $\psi_{\mathbf{p}}^{(-)}(\mathbf{r})$ of the hydrogen atom:

$$\psi_{\mathbf{p}}^{(-)}(\mathbf{r}) = \sum_{l\mu} i^l e^{-i\eta_l(p)} Y_{l\mu}^*(\mathbf{p}) Y_{l\mu}(\mathbf{r}) R_{lp}(r). \quad (6)$$

For the linearly polarized laser pulse and the coordinate system we employ only the terms with $\mu = 0$, of course, actually contribute to the projection. Differential photo-ionization cross-section is computed as $P(\mathbf{p}) = |a(\mathbf{p})|^2$. We are interested in the transverse or lateral electron momentum distribution, describing probability to detect a photo-electron with a given value of the momentum component p_{\perp} perpendicular to the polarization plane. Because of the symmetry of the problem due to the linear polarization of the driving pulse any plane containing polarization vector can be chosen as a polarization plane. Choosing (y, z) -plane as a polarization plane, we obtain for TEMD as function of the lateral momentum $p_{\perp} = p_x$:

$$W(p_{\perp}) = \int P(p_x, p_y, p_z) dp_y dp_z \quad (7)$$

TEMD obtained using this procedure are shown in Figure 1 for two sets of the driving pulse parameters.

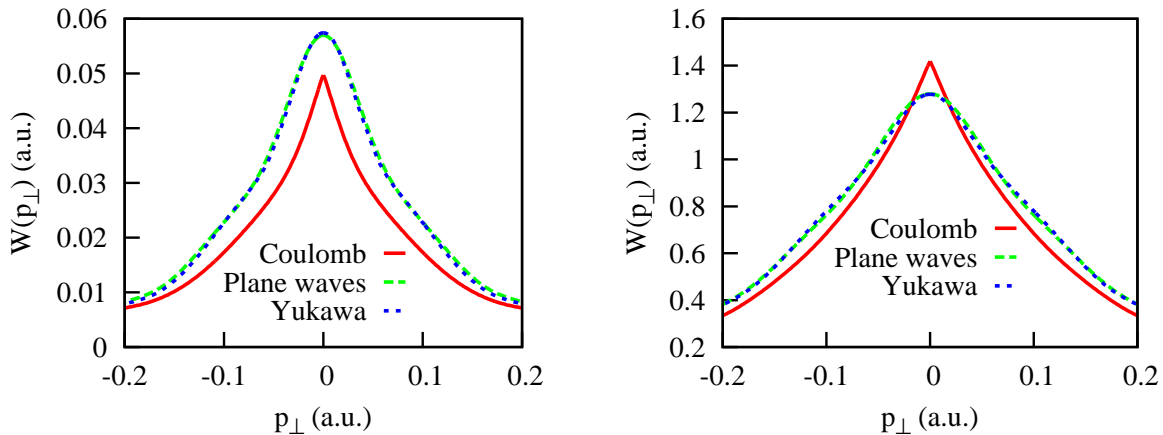


FIG. 1: (Color online) Left panel: TEMD for the laser pulse (4) with pulse intensity of 10^{14} W/cm 2 and total duration of 6 optical cycles. Right panel: the same for the field intensity of 3.5×10^{14} W/cm 2 and pulse duration of 4 optical cycles. Solid (red) line- projection on the ingoing Coulomb scattering states (6). Dash (green)- projection on the basis of plane waves. Short dash (blue)- projection on the set of the ingoing scattering states of the Yukawa potential.

Distributions obtained following the prescription described above and using the Coulomb ingoing scattering states (6) for the projection operation (solid lines in Figure 1) show the cusp-like behavior at $p_{\perp} = 0$. While the TEMD remains continuous at this point, its derivative suffers discontinuity. It was suggested in [13] that cusp originates from the singularity of the Coulomb continuum wave-function at zero energy. We subsequently found some numerical evidence [14] supporting this statement. What interests us in the present work is elucidating the nature of the cusp and the precise type of the discontinuity which the lateral distribution has at $p_{\perp} = 0$. As we shall see, some analytical results describing the discontinuity can be obtained.

We begin by presenting results of a few numerical experiments. We make sure first that the cusp is indeed due to the projection on the set of the Coulomb continuum wave-functions. In Figure 1 we present results obtained if the same solutions of the TDSE at the end of the laser pulse are projected on the set of the plane-waves and the ingoing states of the Yukawa potential $V(r) = -e^{-0.1r}/r$ instead of the Coulomb scattering states. The spectra obtained by using plane-waves basis and scattering states of the Yukawa potential, though agreeing quantitatively rather well with the spectrum obtained by projecting solution of the TDSE on the Coulomb scattering states, show no cusp-like behavior at $p_{\perp} = 0$. The cusp arises, therefore, as a result of the projection operation using the Coulomb scattering states as was surmised in [13]. The question which interests us is

the detailed mechanism responsible for the appearance of the cusp.

We note first that cusp cannot be introduced by the integration procedure, when overlaps between the TDSE solution and the Coulomb scattering states are computed. The amplitude functions $f_l(r, T_1)$ in the expansion of the TDSE solution (5) are square-integrable functions with typical spatial extent corresponding to the distance the outgoing electron wave-packet can have traveled by the end of the laser pulse. Integration of such functions cannot introduce any low-energy singular behavior. Indeed, we can consider that to a good approximation the amplitude functions $f_l(r, T_1)$ have finite support, being non-zero only in the finite region of space (this is what they are in the numerical calculation anyway). Integration of such functions cannot introduce any new singularities which are not already present in the integrand. We must, therefore, look carefully at the singularities present in the Coulomb scattering state (6).

There are two factors in Eq. (6) we have to examine: the Coulomb scattering phase-shifts and the radial Coulomb wave-functions. Explicit expression for the Coulomb phase-shifts reads [19]:

$$\eta_l(p) = \arg \Gamma \left(l + 1 - \frac{i}{p} \right), \quad (8)$$

and it exhibits a highly singular behavior at $p = 0$. On the other hand, the radial functions $R_{lp}(r)$ in Eq. (6) can be written (we use the $\delta(\mathbf{p} - \mathbf{p}')$ normalization) as [19]:

$$R_{lp}(r) = \beta(p) \gamma(p) g_{lp}(r), \quad (9)$$

where

$$\gamma(p) = \frac{1}{1 - e^{-\frac{2\pi}{p}}}, \quad (10)$$

and

$$\beta(p) = \frac{1}{\sqrt{p}}. \quad (11)$$

The function $g_{lp}(r)$ can be found as the solution of the radial Schrödinger equation satisfying a boundary condition $g_{lp}(r) \rightarrow C_l e^{l+1}$ when $r \rightarrow 0$ and C_l is a constant factor independent of energy. By the well-known Poincare theorem $g_{lp}(r)$ is, therefore, an entire function of energy, i.e. an entire function of p^2 . The radial wave-function in (6) is singular at $p = 0$ only due to the presence of the factors $\gamma(p)$ and $\beta(p)$ given by Eq. (10) and Eq. (11).

We have identified, thus, three potential culprits which may introduce singular low-energy behavior and which may be responsible for the formation of a cusp. Let us study them one by one.

Consider first the effect of the Coulomb scattering phase-shift. In Figure 2 we present results of a simple numerical experiment obtained if in the expression for the Coulomb ingoing scattering state (6) we put $\eta_l(p) = 0$ in the exponential function (and use the correct Coulomb radial wave-functions $R_{lp}(r)$).

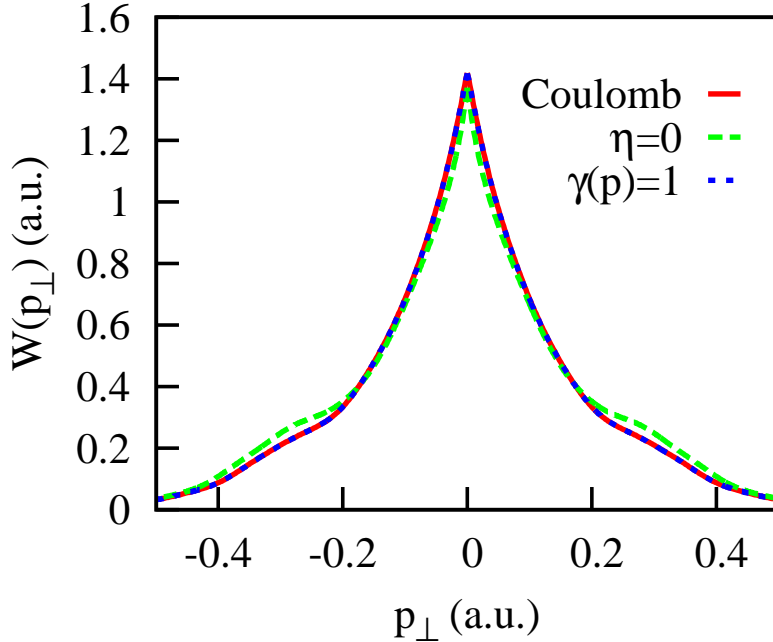


FIG. 2: (Color online) Left panel: TEMD for the laser pulse (4) with pulse intensity of 3.5×10^{14} W/cm² and pulse duration of 4 optical cycles. Solid (red)- projection on the correct ingoing Coulomb states (6). Dash (green)- projection on the set of states (6) with $\eta_l(p) = 0$. Short dash (blue)- projection on set of the states (6) with $\gamma(p) = 0$.

One can see that removal of the scattering phase-shifts $\eta_l(p)$ from the Eq. (6) hardly produces any effect on the lateral spectrum. We could, in fact, anticipate this. Indeed, from the expression for the Coulomb phase-shifts (8) and elementary properties of the Gamma-function one can easily deduce the relation: $\eta_{l+1}(p) = \eta_l(p) - \frac{\pi}{2} + O(p)$ and hence:

$$\eta_{l+1}(p) = \eta_0(p) - \frac{(l+1)\pi}{2} + O(p) , \quad (12)$$

valid when $p \rightarrow 0$. We see, thus, that at low energies the effect of the Coulomb phase-shifts

$\eta_l(p)$ in Eq. (6) reduces to introducing an energy-independent phase-factors for different terms in the sum in Eq. (6), and overall dependence of the photo-ionization amplitude on the $\eta_0(p)$, which cancels out when we compute the squared modulus of the amplitude. On the other hand, with increasing energy Coulomb phase-shifts decrease fast, which explains the fact that Coulomb phase-shifts have virtually no effect on the TEMD. The role of the factor $\gamma(k)$ is equally insignificant as can be seen from Figure 2, where we show the spectrum obtained if we put $\gamma(p) = 1$ in the Eq. (6). Again, this fact could be anticipated, since this factor, though singular at $p = 0$, does not blow up at this point and tends to be one with increasing energy.

We are left, therefore, with the only factor in the Eq. (6) which blows up at $p = 0$, the factor $\beta(p)$ in Eq. (11). There are, of course, other factors in Eq. (6) which are singular at $p = 0$. The spherical harmonics $Y_{l\mu}(p)$ are, strictly speaking, singular functions of the components of the vector \mathbf{p} at $\mathbf{p} = 0$ because of the coordinate system singularity at this point. Similarly, the higher order terms in Eq. (12) are proportional to p , and, in a strict mathematical sense the function p is singular at $\mathbf{p} = 0$ as a function of the components of the vector \mathbf{p} . These singularities are, however, only mild ones, in particular they do not lead to the unbounded growth of the function. The only singularity which does lead to such a growth is the one due to the factor $\beta(p)$.

We are now in a position to elucidate the nature of the cusp in the lateral distribution. To this end, let us note that because of the symmetry of the problem the differential photo-ionization cross-section $P(\mathbf{p})$ is, in fact, a function of two variables only: $P(\mathbf{p}) = P(p, \cos \theta)$, where θ is the angle between electron momentum \mathbf{p} and the z -axis. Expanding this expression in powers of θ we may write for the differential cross-section:

$$P(\mathbf{p}) = \sum_{n=0}^{\infty} P_n(p) \cos^n \theta, \quad (13)$$

where $P_n(p)$ are functions of p only. Coefficients of this expansion can be computed numerically from the known solution of the TDSE by re-expanding products of the spherical harmonics $Y_{l\mu}(p)$ occurring in the expression for the squared modulus of the amplitude $|a(\mathbf{p})|^2$ in series of spherical harmonics with the help of the well-known formulas, and re-expanding in turn the resulting spherical harmonics in powers of $\cos \theta$. Important point here is that coefficients $P_n(p)$ depend only on p and inherit from the amplitudes the singular behavior at $p = 0$ due to the factor $\beta(p)$ in Eq. (11). The $p^{-\frac{1}{2}}$ singular behavior of the amplitudes at $\mathbf{p} = 0$ clearly entails the p^{-1} singular behavior of the coefficients $P_n(p)$ at $p = 0$. Integrating Eq. (13) over the (p_y, p_z) -plane (only terms

with even n give nonzero contributions, of course) we obtain for the TEMD:

$$W(p_\perp) = \sum_{n=0,2,\dots}^{\infty} W_n(p_\perp), \quad (14)$$

where

$$W_n(p_\perp) = \int_0^\infty dq \int_0^{2\pi} d\phi q P_n(p) \left(\frac{q \cos \phi}{p} \right)^n q = \frac{2\pi n!}{\Gamma(n/2 + 1)^2 2^{n-1}} \int_0^\infty dq P_n(p) \frac{q^{n+1}}{(p_\perp^2 + q^2)^{\frac{n}{2}}}, \quad (15)$$

where $p = \sqrt{p_\perp^2 + q^2}$, and we used a cylindrical coordinate system (q, ϕ) in the (p_y, p_z) -plane.

Using Eq. (15) we can obtain asymptotic behavior of $W_n(p_\perp)$ for $p_\perp \rightarrow 0$. As we mentioned above $P_n(p)$ behave as p^{-1} for small energies. Let us choose some small positive Q and represent $P_n(p)$ in the interval $(0, Q)$ as $P_n(p) = C_n/p + P'_n(p)$ where $P'_n(p)$ is non-singular at $p = 0$. Singular behavior of the integrals in Eq. (15) at $p_\perp = 0$ can appear only as a result of the integration of the singular term C_n/p in $P_n(p)$ over the interval $(0, Q)$. Indeed, the integrands in both integral over the interval $(0, \infty)$ with $P'_n(p)$ and the integral over the interval (Q, ∞) with C_n/p contain smooth regular functions as integrands which cannot lead to a small- p_\perp singular behavior. We can write, therefore:

$$W_n(p_\perp) = C_n I_n(p_\perp, Q) + W_n^{\text{reg}}(p_\perp), \quad (16)$$

where

$$I_n(p_\perp, Q) = \int_0^Q dq \frac{q^{n+1}}{(p_\perp^2 + q^2)^{\frac{n+1}{2}}}, \quad (17)$$

C_n is a constant, and $W_n^{\text{reg}}(p_\perp)$ are non-singular at $p_\perp = 0$, behaving near this point as $W_n^{\text{reg}}(p_\perp) \approx u_n^0 + u_n^2 p_\perp^2$ with some constant u_n^0 and u_n^2 .

It is clear from Eq. (17) why this contribution becomes singular at $p_\perp = 0$. While the integral has a finite value if we put $p_\perp = 0$, an attempt to calculate the derivative with respect to p_\perp by differentiating under the integral sign leads to a divergent expression. We have to be more careful in evaluating asymptotic of the integral. Using well-known formulas for the integral representation and asymptotic properties of the hypergeometric function $F(a, b; c; z)$ [20] we obtain:

$$I_n(p_\perp, Q) = \frac{Q^{n+2}}{2|p_\perp|^{n+1}} \frac{\Gamma(\frac{n}{2}+1) \Gamma(\frac{1}{2})}{\Gamma(\frac{n}{2}+\frac{3}{2})} F\left(\frac{n+1}{2}, \frac{n}{2}+1; \frac{n}{2}+\frac{3}{2}; -\frac{Q^2}{p_\perp^2}\right) \approx A_n + B_n |p_\perp| \quad p_\perp \rightarrow 0, \quad (18)$$

where we do not give explicit expressions for the unimportant constant factors.

From Eq. (16) and Eq. (18) we conclude that $W_n(p_\perp)$ behave for small p_\perp as linear functions of $|p_\perp|$:

$$W_n(p_\perp, Q) = g_n + h_n |p_\perp| + O(p_\perp^2) \quad p_\perp \rightarrow 0, \quad (19)$$

where g_n, h_n are some constants. This implies the following cusp structure of $W_n(p_\perp)$ at $p_\perp = 0$. First derivative of $W_n(p_\perp)$ with respect to p_\perp is discontinuous at $p_\perp = 0$, the second derivative is, therefore, infinite. That this formula indeed reproduces asymptotic behavior correctly, can be seen from Figure 3. The contributions $W_n(p_\perp)$ as functions of lateral momentum obtained from the TDSE calculation are shown in Figure 3. $W_n(p_\perp)$ vary considerably with n in magnitude and need not be positive, to facilitate the comparison we present the scaled contributions: $W_n(p_\perp)/|W_n(0)|$. In Figure 3 we present also the results of the linear fits: $W_n(p_\perp)/|W_n(0)| = A + B|p_\perp|$.

Two features are apparent from Figure 3. First, for small values of p_\perp the contributions $W_n(p_\perp)$ are indeed linear functions of $|p_\perp|$ in agreement with the asymptotic estimate (19) we made above. Second, the region where this asymptotic estimate represents $W_n(p_\perp)$ accurately shrinks with n . There is, of course, nothing unusual in such behavior. Asymptotic estimates give us asymptotic behavior for small values of a parameter, but they do not necessarily tell us how small the parameter should be for the estimate to be accurate. A glance at the behavior of the integrals in Eq. (17) as functions of lateral momentum may help us to understand what is happening. We show in Figure 4 integrals $I_n(p_\perp, Q)$ as functions of p_\perp for a fixed value of $Q = 0.05$ a.u. Figure 4 shows qualitatively the behavior similar to what we observe in Figure 3, the region where the asymptotic expression represents $I_n(p_\perp, Q)$ accurately shrinks with n . Thus, the behavior of $W_n(p_\perp)$ is a consequence of the property of the integrals $I_n(p_\perp, Q)$ that the region where linear in $|p_\perp|$ asymptotic takes over shrinks progressively with n .

This feature of $W_n(p_\perp)$ is quite important for understanding how the cusp in TEMD is produced. As Eq. (19) shows the terms of the series (14) behave as linear functions of $|p_\perp|$ for small enough p_\perp . At first glance, that would suggest that the sum of the series (14), the TEMD $W(p_\perp)$, would exhibit the same behavior linear in $|p_\perp|$ near $p_\perp = 0$. That would imply the following

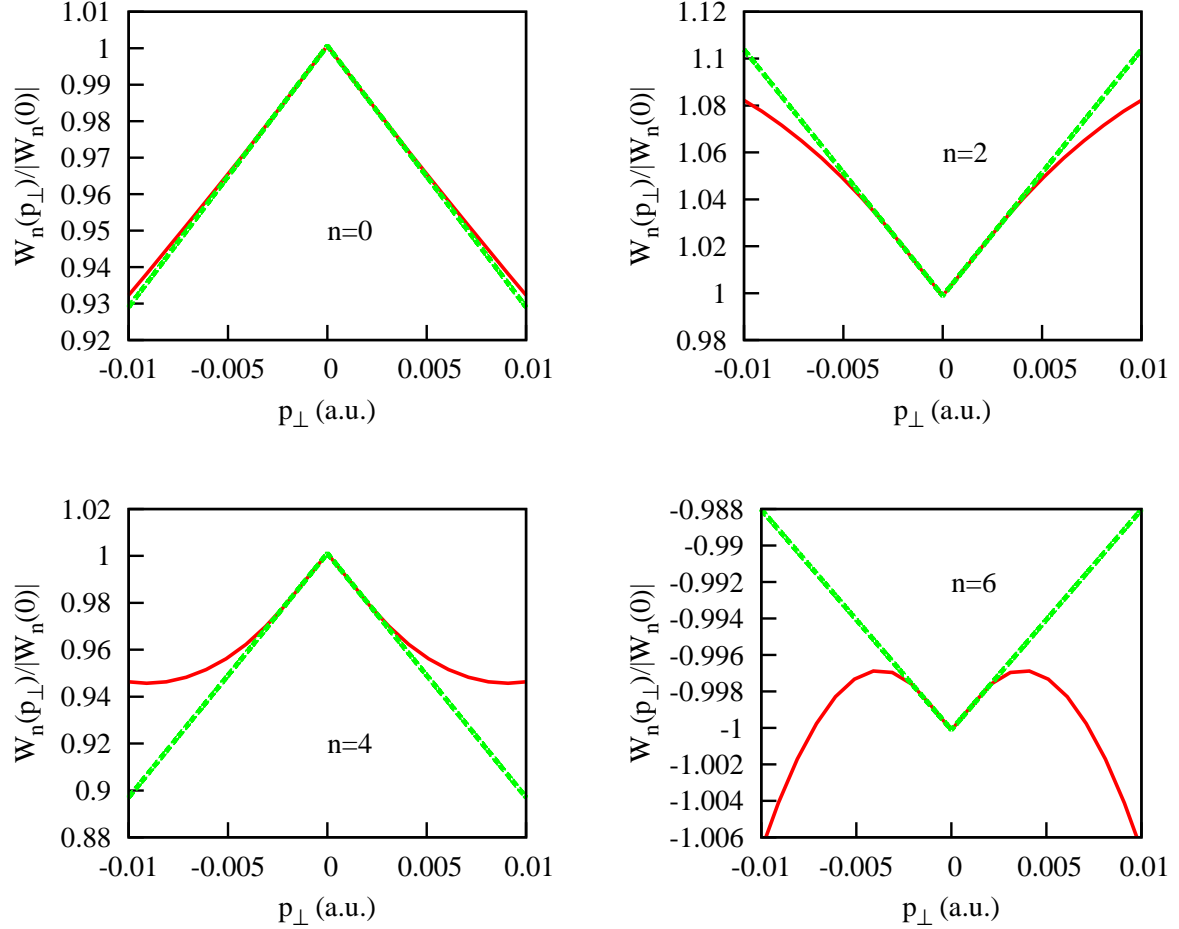


FIG. 3: (Color online). Solid (red) line: scaled terms of the series (14) $W_n(p_\perp)/|W_n(0)|$ as functions of lateral momentum p_\perp . Dash (green): linear fit: $W_n(p_\perp)/|W_n(0)| = A + B|p_\perp|$. Field intensity 3.5×10^{14} W/cm², pulse duration four optical cycles.

cusp structure: TEMD would have discontinuous first and infinite second derivative at $p_\perp = 0$. On the other hand, the cusps shown in Figure 1 look more like functions of p_\perp with infinite first derivative. In other words $W(p_\perp)$ grows visibly faster than $|p_\perp|$ near $p_\perp = 0$. This apparent contradiction is resolved when one realizes that $W(p_\perp)$ is a sum (14) of the terms $W_n(p_\perp)$. Each of $W_n(p_\perp)$ behaves as a linear function of $|p_\perp|$ in some vicinity of $p_\perp = 0$, but, as we saw above, the interval of p_\perp on which linear dependence is a good approximation shrinks with n . If, as Figure 3 suggests, outside the interval of applicability of the asymptotic law the $W_n(p_\perp)$ grow slower with p_\perp (we see this behavior for the integrals $I_n(p_\perp, Q)$ in Figure 4), the sum of all $W_n(p_\perp)$ in (14) will exhibit precisely the behavior seen in Figure 1- the growth which is faster than linear for $p_\perp \rightarrow 0$. With $p_\perp \rightarrow 0$ the terms with higher n switch progressively from the relatively slow growth outside

the asymptotic region to a faster growth linear in $|p_\perp|$, once p_\perp is inside the region of the validity of the asymptotic law (19) for a particular n .

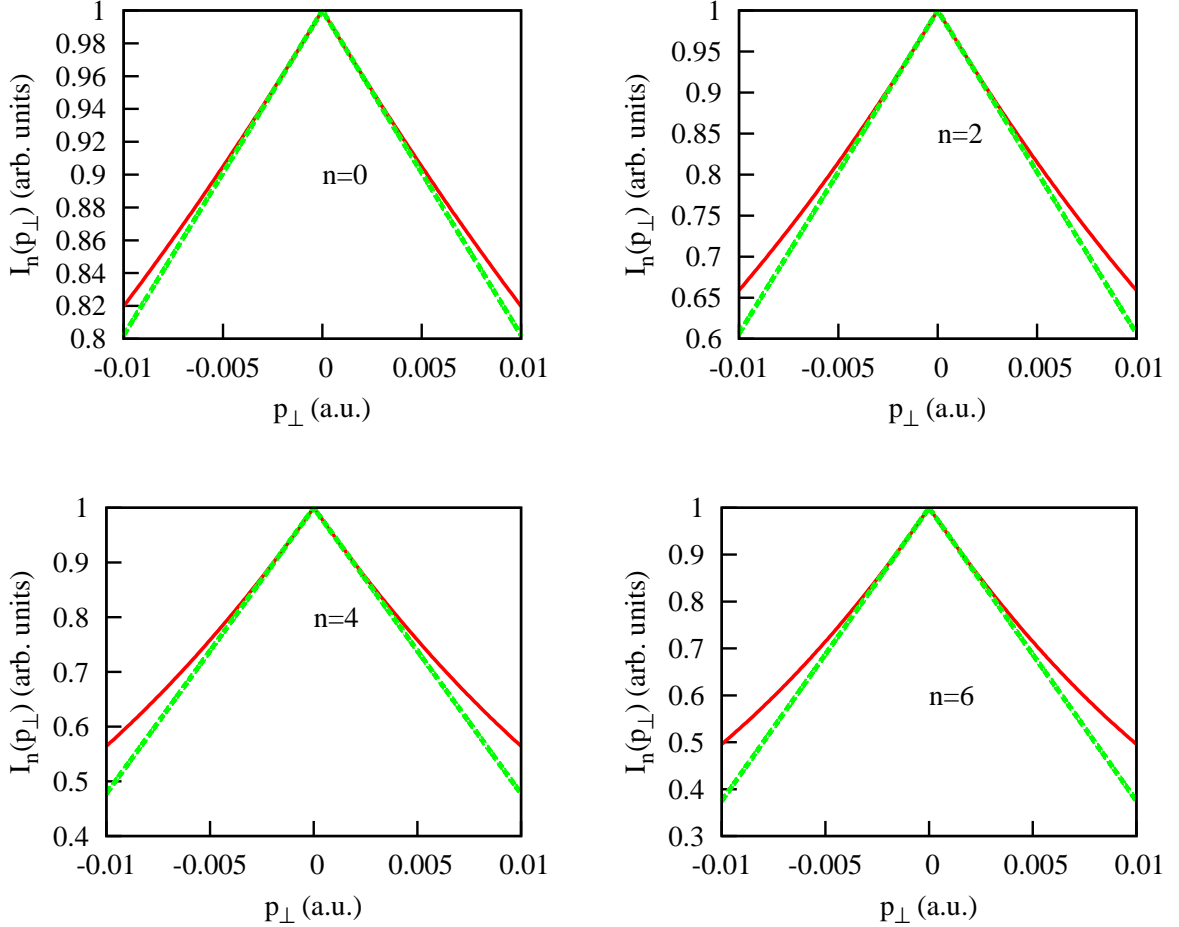


FIG. 4: (Color online) Solid (red) line: Integrals $I_n(p_\perp, Q)$ as functions of lateral momentum p_\perp for $Q = 0.05$. Dash (green): linear fit: $I_n(p_\perp, Q) = A + B|p_\perp|$.

To see this quantitatively let us use a simple example. Suppose that for the coefficients C_n in Eq. (16) we have $C_n = c^n$ with some constant c . For the sum of the series (14) we would have then (we omit the contribution of the regular parts $W_n^{\text{reg}}(p_\perp)$ since they do not lead to the singular behavior):

$$I(p_\perp) = \sum_{n=0,2,\dots}^{\infty} \int_0^Q dq \frac{q^{n+1}}{(p_\perp^2 + q^2)^{\frac{n+1}{2}}} = \int_0^Q \frac{pq}{p_\perp^2 + q^2} dq, \quad (20)$$

where $p = \sqrt{p_\perp^2 + q^2}$. Asymptotic behavior of the integral on the r.h.s of Eq. (20) for small p_\perp can easily be found. The results reads:

$$I(p_\perp, Q) = A + B|p_\perp| \ln |p_\perp| \quad p_\perp \rightarrow 0, \quad (21)$$

with some constants A and B . We see, thus, that while terms of the series (20) all have $|p_\perp|$ -cusps at $p_\perp = 0$, the sum of the series (20) exhibits more singular cusp-like behavior at this point. For the terms of series (20) the first derivatives with respect to p_\perp are discontinuous at $p_\perp = 0$ and the second derivative is infinite at $p_\perp = 0$. The cusp-singularity of the sum of the series (20) is more severe, the first derivative with respect to p_\perp is infinite at $p_\perp = 0$. This behavior of $I(p_\perp, Q)$ in Eq. (21) and its first derivative is illustrated in Figure 5.

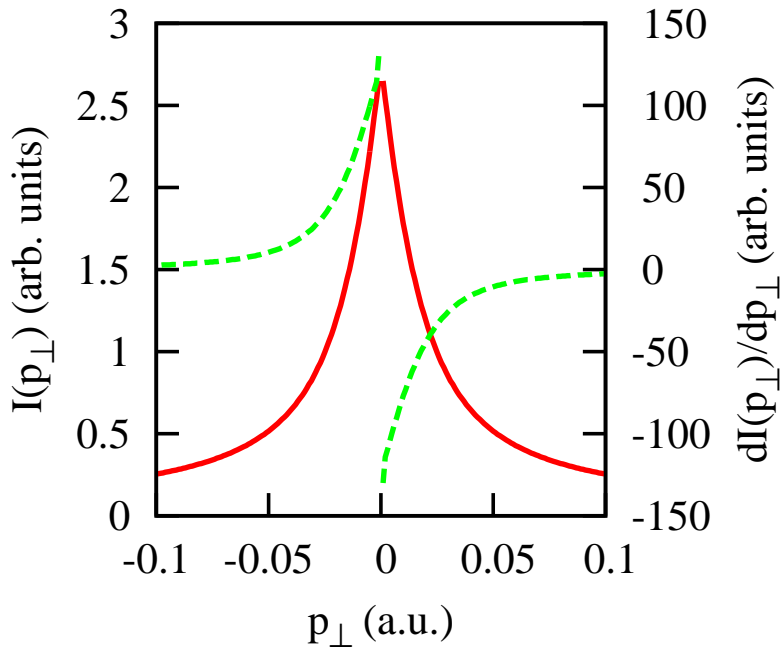


FIG. 5: (Color online) Sum of the series (20) and its first derivative near $p_\perp = 0$ for $Q = 0.05$. Solid (red) line: sum of the series (20). Dash (green): its first derivative.

Incidentally, the asymptotic law (21) reproduces fairly well the TEMD obtained in our TDSE calculations. As one can see from Figure 6, the two-parameter formula $A + B|p_\perp| \ln |p_\perp|$ (A and B considered as fitting parameters) gives actually better results than the three-parameter fit based on the equation: $W(p_\perp) = A + B|p_\perp|^\alpha$ (A , B and α as fitting parameters). We cannot, of course, claim that $A + B|p_\perp| \ln |p_\perp|$ is the actual behavior of the TEMD $W(p_\perp)$ for small p_\perp . As we saw, to describe the cusp in the TEMD we rely on two ingredients. We need first to describe small- p_\perp behavior of the "partial" distributions $W_n(p_\perp)$ in the (14). Eq. (16) and Eq. (18) provide an answer

to this problem. To find small- p_{\perp} behavior of the sum of the series (14) we also need to know the weights with which different $I_n(p_{\perp})$ in Eq. (16) contribute to the sum- the coefficients C_n in this equation. It is clear that to establish small- p_{\perp} behavior of the sum of the series (14) we actually need to know only the large- n asymptotic behavior of C_n . The logarithmic behavior in Eq. (21) obtains, in particular, assuming that C_n form a geometric sequence, a plausible assumption leading to apparently satisfactory results, which we, however, did not prove, so we may regard this formula as a plausible, perhaps, but only a tentative expression.

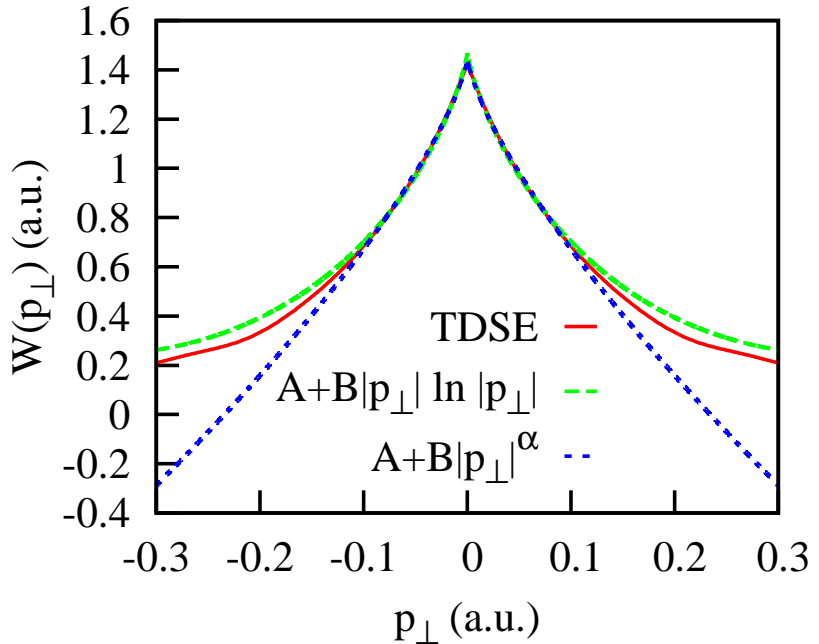


FIG. 6: (Color online) TEMD for the field intensity of 3.5×10^{14} W/cm² and pulse duration of 4 optical cycles. Solid (red) line: TDSE calculation. Dash (green): fit based on the equation: $W(p_{\perp}) = A + B|p_{\perp}| \ln |p_{\perp}|$ (fitting parameters A and B). Short dash (blue): fit based on the equation: $W(p_{\perp}) = A + B|p_{\perp}|^{\alpha}$ (fitting parameters A , B and α).

III. CONCLUSION

We considered in detail the formation of the cusp in the TEMD for the process of strong field ionization. As we saw, one can push analytic approach to this problem quite far. Our starting point was the series (14) resulting from the expansion of the differential probability in the powers

of $\cos \theta$ - the angle between the polarization vector and the electron momentum. We were able to show that the terms $W_n(p_\perp)$ of this series behave as linear functions of $|p_\perp|$ for small p_\perp . This behavior is a consequence of the properties of the Coulomb continuous spectrum wave-functions, and is present, therefore, for any system regardless of what the actual Hamiltonian is, as long as the wave-function of the system after the end of the laser pulse is projected on the set of the Coulomb wave-functions. If this were the whole story the TEMD would have the $|p_\perp|$ -cusp at $p_\perp = 0$. For such a cusp the first derivative at $p_\perp = 0$ is discontinuous, and the second derivative is infinite.

There is, however, the second step we have to perform to obtain the TEMD. The functions $W_n(p_\perp)$ in (14) with the small- p_\perp asymptotic which we established in Eq. (19), constitute the building blocks from which TEMD can be build by summing up the expansion (14). It is at this stage, where dynamic information, i.e. the information about particular details of the ionization process, ultimately encapsulated in the solution of the TDSE, becomes important. The "partial" lateral distributions $W_n(p_\perp)$ considered as functions of n enter the series (14) with different weights. Mathematically, it is reflected in the Eq. (16) which represents $W_n(p_\perp)$ as a product of the integral $I_n(p_\perp)$ and a coefficient C_n which is a function of n only. Coefficients C_n depend, of course, on the dynamics of the system, since they result ultimately from the projection of the TDSE wave-function at the end of the laser pulse. As we saw, the summation procedure can make the character of the cusp for the sum of the series (14) different from the linear $|p_\perp|$ -cusp which each of the terms of the series exhibits at $p_\perp = 0$. The reason for this is, roughly speaking, the fact that for the terms of the series (14) with higher n the region of lateral momenta for which linear in $|p_\perp|$ asymptotic law holds for $W_n(p_\perp)$ shrinks, or in stricter mathematical language, the fact that the small- p_\perp asymptotic (19) for $W_n(p_\perp)$ is non-uniform in n .

To summarize, we demonstrated that the cusp in the TEMD arises as a consequence of two factors: The singularity of the Coulomb wave-function produces a simple cusp of the $A + Bp_\perp$ type. The view expressed in [13] that cusp is due to the singularity of the Coulomb scattering state is, therefore, basically correct, the Coulomb wave-function is responsible for the presence of the cusp. This fact has nothing to do whatsoever with dynamics of the photo-ionization process. The character of the cusp we observe in the TEMD, however, may differ from the $A + Bp_\perp$ -type created by the Coulomb wave-function. The origin of this difference lies in the dynamics, it is ultimately due to the properties of the coefficients of the expansions (13), (14), which depend on the wave-function at the end of the laser pulse.

IV. ACKNOWLEDGMENTS

This work was supported by the Institute for Basic Science under IBS-R012-D1.

[1] L. V. Keldysh, Sov. Phys. -JETP **20**, 1307 (1965).

[2] F. H. M. Faisal, J. Phys. B **6**, L89 (1973).

[3] H. R. Reiss, Phys. Rev. A **22**, 1786 (1980).

[4] A. M. Perelomov, V. S. Popov, and M. V. Terentiev, Sov. Phys. -JETP p. 924 (1966).

[5] M. V. Ammosov, N. B. Delone, and V. P. Krainov, Sov. Phys. -JETP p. 1191 (1986).

[6] V. S. Popov, Physics-Uspekhi **47**, 855 (2004).

[7] S. V. Popruzhenko, Journal of Physics B: Atomic, Molecular and Optical Physics **47**, 204001 (2014).

[8] N. I. Shvetsov-Shilovski, D. Dimitrovski, and L. B. Madsen, Phys. Rev. A **85**, 023428 (2012).

[9] R. Boge, C. Cirelli, A. S. Landsman, S. Heuser, A. Ludwig, J. Maurer, M. Weger, L. Gallmann, and U. Keller, Phys. Rev. Lett. **111**, 103003 (2013).

[10] A. N. Pfeiffer, C. Cirelli, A. S. Landsman, M. Smolarski, D. Dimitrovski, L. B. Madsen, and U. Keller, Phys. Rev. Lett. **109**, 083002 (2012), URL <http://link.aps.org/doi/10.1103/PhysRevLett.109.083002>.

[11] S. V. Popruzhenko, JETP **145**, 580 (2014).

[12] L. Arissian, C. Smeenk, F. Turner, C. Trallero, A. V. Sokolov, D. M. Villeneuve, A. Staudte, and P. B. Corkum, Phys. Rev. Lett. **105**, 133002 (2010).

[13] A. Rudenko, K. Zrost, T. Ergler, A. B. Voitkiv, B. Najjari, V. L. B. de Jesus, B. Feuerstein, C. D. Schröter, R. Moshammer, and J. Ullrich, Journal of Physics B: Atomic, Molecular and Optical Physics **38**, L191 (2005), URL <http://stacks.iop.org/0953-4075/38/i=11/a=L01>.

[14] I. A. Ivanov, Phys. Rev. A **90**, 013418 (2014).

[15] I. A. Ivanov, A.S.Kheifets, J. Calvert, S. Goodall, X. Wang, H. Xu, A. Palmer, D. Kielpinski, I. Litvinyuk, and R.T.Sang, ArXiv e-prints p. 1503.04891 (2015), URL <http://arxiv.org/abs/1503.04891>.

[16] I. A. Ivanov, Phys. Rev. A **83**, 023421 (2011).

[17] I. A. Ivanov and A. S. Kheifets, Phys. Rev. A **87**, 033407 (2013).

[18] M. Nurhuda and F. H. M. Faisal, Phys. Rev. A **60**, 3125 (1999).

- [19] L. D. Landau and E. M. Lifshitz, *Quantum Mechanics* (Pergamon Press, 1965).
- [20] M. Abramowitz and I. E. Stegun, *Handbook of Mathematical Functions* (National Bureau of Standards, Washington, 1967).